High-resolution insights into episodes of crystallization, hydrothermal alteration and remelting in the Skaergaard intrusive complex

Jörn-Frederik Wotzlaw [a,*], Ilya N. Bindeman [a,b], Urs Schaltegger [a], C. Kent Brooks [c], H. Richard Naslund [d]

[a] Section of Earth and Environmental Sciences, University of Geneva, Rue des Maraichers 13, CH-1205 Geneva, Switzerland
[b] Department of Geological Sciences, University of Oregon, Eugene, OR 97403, USA
[c] Natural History Museum of Denmark, University of Copenhagen, Øster Voldgarde 5-7, DK-1350 Copenhagen, Denmark
[d] Department of Geological Sciences, Binghamton University, PO BOX 6000, Binghamton, NY 13902, USA

ARTICLE INFO

ABSTRACT

This paper presents a new high-precision zircon U–Pb geochronological view on the crystallization and assembly process of one of the most important and intensely studied intrusive bodies on Earth—the Skaergaard intrusion in East Greenland. With analytical uncertainties of a few tens of thousands of years, we were able to resolve several important events during cooling of this intrusion.

Initial cooling of the shallowly intruded ~ 300 km^3 of tholeiitic basaltic magma from liquidus to zircon saturation at ~ 1000 °C is recorded by a precise zircon crystallization age of 55.960 ± 0.018 Ma of an intercumulus gabbroic pegmatite in the lower portion of the intrusion. Based on this zircon crystallization age and a published cooling model we estimate the "true" age of emplacement to be ~ 56.02 Ma. The last portions of Skaergaard appear to crystallize completely ~ 100 ka after emplacement as recorded by abundant ~ 55.91–55.93 Ma zircons in the Sandwich Horizon (SH), where lower and upper solidification fronts met. Intrusion of an isotopically distinct new magma batch, the ~ 600 m thick Basistoppen Sill, into the solidified upper portion of Skaergaard, happened at 55.895 ± 0.018 Ma, suggesting close timing between crystallization of evolved rocks around the SH and intrusion of the Basistoppen Sill. The novel result of this work is the demonstration that zircons in the SH, > 100 m below the Basistoppen contact, have a bimodal age distribution, with the youngest population of 55.838 ± 0.019 Ma postdating intrusion of the Basistoppen Sill by 57 ± 37 ka. Oxygen isotope analyses reveal that SH zircons are low and heterogeneous with respect to $\delta^{18}O$. These results support the proposed conclusion that the SH crystallized twice: it was fully crystalline, then hydrothermally-altered by low-$\delta^{18}O$ surface waters and subsequently partially remelted, triggered by heat of the Basistoppen Sill. The low-degree partial melt generated during remelting partially migrated upward by intergranular compaction-driven flow, explaining the existence of the most incompatible trace element rich horizon, ~ 100 m above SH.

As the Skaergaard intrusion is also the most classic example of a shallow meteoric hydrothermal system, this work documents the alternating processes in a life of an intrusion with periods of hydrothermal cooling, heating by new intrusions, and related remelting events, which cause the generation of low-$\delta^{18}O$ magmas.

Our precise temporal framework for intrusion crystallization also provides constraints for the timing of coeval flood basalt volcanism and its synchronicity with the Paleocene-Eocene thermal maximum.

1. Introduction

Chemically-zoned plutons have been the subject of intense research aiming to model the physical mechanisms of igneous differentiation (McBirney and Noyes, 1979; McBirney, 1995; Boudreau and McBirney, 1997; McKenzie, 2011). Most of these models concentrate on the efficiency of crystal-melt separation, the role of convection, and recently silicate liquid immiscibility (Jakobsen et al., 2005, 2010a; Veksler et al., 2007; Humphreys, 2011; Holness et al., 2011). When dealing with now solid plutonic bodies it is important to realize that there are many other time-integrated processes that are possible to unravel with new tools. It is particularly important to realize that even the simplest examples of igneous bodies may contain records of multiple

* Corresponding author. Tel.: +41 22 3796600; fax: +41 22 3793210.
E-mail address: joern.wotzlaw@unige.ch (J.F. Wotzlaw).

refilling events and events of remelting of preexisting rocks that may be traced by radiogenic and/or stable isotopes and the timing of such events can be quantified using precise geochronological methods. In this study we investigate the late-stage evolution of the Skaergaard intrusion aiming to test proposed petrogenetic models and quantify time-scales of late-stage shallow crustal remelting and generation of low-δ^{18}O magmas (Bindeman et al., 2008).

Since its discovery in 1930, the Skaergaard intrusion has been a classic locality for the study of closed-system igneous differentiation (e.g., Wager and Deer, 1939; Wager and Brown, 1968; Brooks et al., 1991; McBirney, 1995; Irvine et al., 1998). After emplacement in the unconformity between the Precambrian basement and overlying Cenozoic basaltic lavas (Fig. 1), it evolved by fractional crystallization from primitive olivine gabbro to Fe-rich ferrodiorite with interstitial granophyre. Progressive crystallization from the floor, walls and roof of the intrusion produced the Layered Series (LS), the Marginal Border Series (MBS) and the Upper Border Series (UBS), respectively (Wager and Deer, 1939). The LS comprises the bulk of the volume and is further subdivided into zones and subzones (Fig. 1c) reflecting the appearance and disappearance of fractionating cumulus phases (Wager and Deer, 1939; Wager and Brown, 1968; Lindsley et al., 1969; Irvine et al., 1998). The upper and lower crystallization fronts coalesced around what is known as the Sandwich Horizon (SH), which contains the most evolved major element differentiation indices (e.g., highest Fe/Mg ratios). However, the highest incompatible trace element concentrations occur tens of meters above the SH,

a layer called the secondary SH (McBirney, 2002), or following Bindeman et al. (2008), the "Brooks" Horizon, labeled after the paper by Brooks (1969) who first discovered this enrichment.

The Skaergaard intrusion is perhaps the simplest layered igneous body on Earth in the sense that ∼300 km³ of tholeiitic basaltic magma formed and intruded in a single event into a shallow (ca. 1–2 km) rift zone during ∼56 Ma North Atlantic extension, and then differentiated from bottom and top by a closed system differentiation process without much mass loss to the surface, and without much assimilation of highly radiogenic Archean country rocks. Recent work has addressed the importance of crystal compaction vs. convective differentiation (Tegner et al., 2009; McKenzie, 2011), the role of igneous layering, and the role of liquid immiscibility (Jakobsen et al., 2005; 2010a; Veksler et al., 2007; Humphreys, 2011; Holness et al., 2011), but does not attempt to challenge the original views of Wager and Deer (1939) about top to bottom, and bottom to top, liquidus to solidus crystallization of Skaergaard.

2. Previous stable isotope studies and geochronology of the Skaergaard intrusion

These canonical differentiation trends observed in Skaergaard were the initial driving force to empirically understand changes of oxygen and hydrogen isotopic fractionation during magmatic differentiation (Taylor and Epstein, 1963). Subsequent studies, however, found that primary magmatic values were nearly
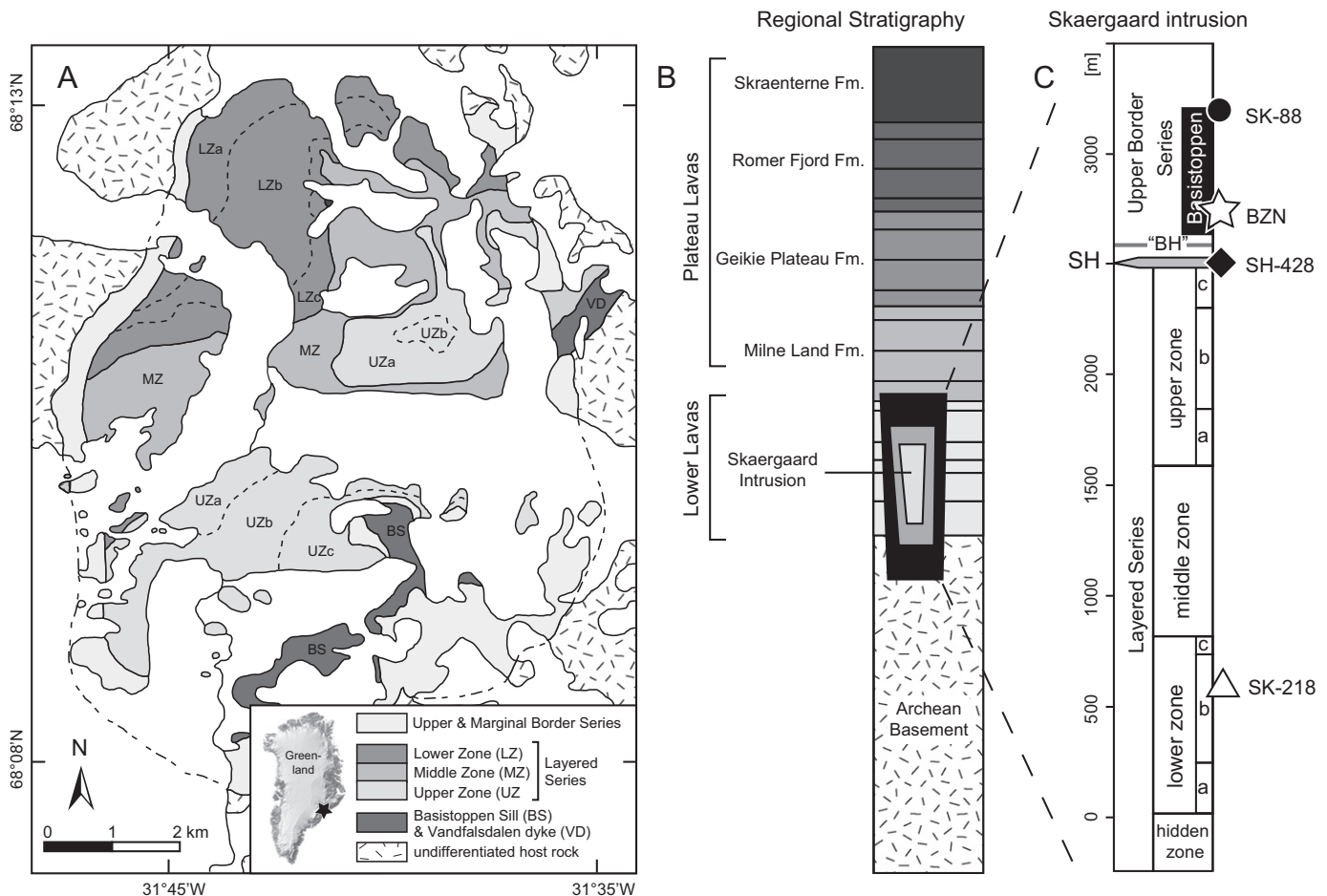

Fig. 1. (A) Geological map of the Skaergaard intrusive complex (McBirney, 1989), (B) regional stratigraphy showing stratigraphic relationship between the Skaergaard intrusion, the Precambrian basement and overlying basalts (after Jakobsen et al., 2010a,b) and (C) stratigraphic column of the Skaergaard intrusion (Wager and Brown, 1968) showing stratigraphic position of analyzed samples. Abbreviations: SH—Sandwich Horizon, BH—Brooks Horizon.

completely overprinted by exchange with low-δ^{18}O meteoric hydrothermal fluids (Taylor, 1968; Taylor and Forester, 1979; Norton et al., 1984) and that the Skaergaard intrusion drove its own shallow meteoric hydrothermal system in the waning stages of intrusion crystallization and during subsolidus cooling. This high temperature hydrothermal alteration of Skaergaard rocks resulted in highly diverse δ^{18}O and δD values of feldspars, secondary micas and other minerals, forming a characteristic bulls-eye pattern of greater alteration centered around the upper portion of the intrusion, where water–rock ratios were the greatest (Taylor and Forester, 1979). Norton and Taylor (1979) numerically modeled this process and estimated that the hydrothermal system lasted $\sim$130 ka, and this estimate remains the best in terms of duration of magmatic-hydrothermal events in Skaergaard.

Recently, Bindeman et al. (2008) reexamined oxygen isotope systematics across the Skaergaard intrusion aiming to identify primary magmatic signatures by laser fluorination analyses of small multigrain fractions, individual phenocrysts and refractory accessory minerals. They confirmed the suggestion by Taylor and Forester (1979) that Skaergaard was initially a normal-δ^{18}O 5.7‰ magma but convincingly demonstrated that late-stage differentiates (ferrodiorites) found around the Sandwich Horizon have crystallized from low-δ^{18}O magmas as they contain diverse low-δ^{18}O populations of zircon, sphene, amphibole and other minerals. As generation of low-δ^{18}O magma in a closed system igneous fractionation is impossible, incorporation of meteoric water derived oxygen into these late state differentiates is required. Bindeman et al. (2008) suggested that generation of these ^{18}O depleted magmas could involve sequestration of low-δ^{18}O melt/fluid from dehydration of hydrothermally altered low-δ^{18}O fallen blocks into the main volume of the intrusion, but favored partial remelting of already solidified and hydrothermally-altered (and thus low-δ^{18}O) rocks, which happened under the Basistoppen intrusion. Complementing these published oxygen isotope data (Bindeman et al., 2008), we here report zircon oxygen isotope ratios measured by ion microprobe to better constrain the magnitude and related mechanisms of ^{18}O depletion of late-stage differentiates.

In contrast to numerous petrologic, geochemical and isotopic studies, surprisingly few geochronological data have been published for the Skaergaard intrusion. Brooks and Gleadow (1977) reported a zircon fission track date of 54.6 ± 1.7 Ma that was later confirmed by biotite and hornblende ^{40}Ar/^{39}Ar dates from transgressive granophyres of 55.40 ± 0.14 and 55.48 ± 0.30 Ma, respectively (Hirschmann et al., 1997). Recently, Hamilton and Brooks (2004) reported an ion microprobe (SHRIMP) zircon ^{206}Pb/^{238}U date of 55.59 ± 0.13 Ma. While these consistent dates appear to constrain the age of emplacement reasonably precisely and put Skaergaard in the broader context of North Atlantic rift opening, they do not yield information about time scales of intraplutonic crystallization and petrologic evolution of the Skaergaard intrusion.

Recent advances in U–Pb geochronology by isotope dilution-thermal ionization mass spectrometry (ID-TIMS), resulting in analytical uncertainties and external reproducibility at the permil level (e.g., Schoene et al., 2006; Sláma et al., 2008), allow the evolution of Cenozoic magmatic systems to be tracked at unprecedented temporal resolution and absolute time constraints to be added to thermal and petrogenetic models (e.g., Schaltegger et al., 2009; von Quadt et al., 2011). Given superb exposure and the young $\sim$56 Ma age of Skaergaard, the ID-TIMS method should in theory permit recognition of individual episodes during $\sim$130 ka duration of Skaergaard crystallization. This work employs chemical abrasion ID-TIMS techniques to obtain the best absolute age for emplacement of the Skaergaard intrusion, to determine the age of its most important coeval magma batch, the tholeiitic Basistoppen sill,

and to explore in detail the crystallization and remelting history of the Sandwich Horizon, as well as the petrogenesis of the Brooks Horizon. In particular, we discuss how late intrusion of the Basistoppen Sill lead to remelting of already crystallized Skaergaard differentiates that resulted in the appearance of low-δ^{18}O magmas around SH. We also model how intergranular melt flow during the proposed remelting event could have generated the Brooks Horizon, the most incompatible trace element rich horizon in Skaergaard. We further discuss the bearing of our temporal framework of intrusion crystallization on the timing of intimately linked flood basalt volcanism and the temporal relationship with environmental perturbations at the Paleocene–Eocene boundary.

3. Materials and methods

Zircons were earlier separated from ferrodiorites of the Sandwich Horizon (SH-428; Hamilton and Brooks, 2004), a podiform gabbroic pegmatite from lower zone b of the layered series (SK-218; Larsen and Brooks, 1994), the post-Skaergaard tholeiitic Basistoppen Sill (BZN) and the related Sydtoppen granophyre (SK-88; Naslund, 1989). A total of 32 zircon crystals from samples SK-218, SH-428, and BZN were analyzed as single grains by ID-TIMS at the University of Geneva following procedures of Schoene et al. (2010). Prior to dissolution, all crystals were annealed by heating to 900 °C for 48 h in a muffle furnace, transferred into 3 ml Savillex beakers and chemically abraded in HF+trace HNO_3 at 180 °C for 15 h in Parr bombs (Mattinson, 2005). Subsequently, zircons were rinsed with water, fluxed for several hours in 6 N HCl and ultrasonically cleaned with water, acetone and 3 N HNO_3. Single crystals were loaded in 200 μl Savillex capsules, spiked with $\sim$3–5 mg of the EARTHTIME ($\pm^{202}$Pb)-^{205}Pb-^{233}U-^{235}U tracer solution (http://www.earth-time.org/) and dissolved in $\sim$70 μl HF at 210 °C for 48 h in Parr bombs. After dissolution, samples were dried down and redissolved in 6 N HCl at 180 °C overnight, dried down again and redissolved in 3 N HCl. U and Pb were separated using a modified HCl-based single-column anion exchange chemistry (Krogh, 1973). The Zr, Hf, and trace element fraction ("wash") was collected for Hf isotope analyses (see below). The U–Pb fraction was loaded on outgassed Re filaments with a Si-Gel emitter modified from Gerstenberger and Haase (1997). U and Pb isotopic measurements were performed on a Thermo TRITON thermal ionization mass spectrometer. Pb was measured in dynamic mode on a MasCom secondary electron multiplier. Analyses employing the ET2535 tracer were corrected using the fractionation factor derived from the measured ^{202}Pb/^{205}Pb ratio assuming a true value of 0.99924. Measurements employing the ET535 tracer were corrected for $0.13 \pm 0.02\%$/amu mass fractionation based on >200 analyses using the ^{202}Pb-^{205}Pb double spike performed during the course of this study. U was measured as U-oxide in static mode on Faraday cups equipped with 10^{12} Ω resistors. Measured isotopic ratios were corrected for interferences of ^{233}U^{18}O^{16}O on ^{235}U^{16}O$_2$ using an ^{18}O/^{16}O of 0.00205, measured on large U500 loads, and for mass fractionation using the measured ^{233}U/^{235}U ratio relative to a value of 0.99506 for both tracers. All common Pb in the zircon analyses (average: 0.62 ± 0.14 pg) was assumed to be procedural blank. U–Pb ratios and dates were calculated relative to a ^{235}U/^{205}Pb ratio of $100.23 \pm 0.023\%$ (1σ) and raw data were reduced using Tripoli and U–Pb_Redux software (Bowring et al., 2011) that employs algorithms of McLean et al. (2011). All uncertainties are reported at the 95% confidence level and exclude systematic uncertainties associated with tracer calibration and decay constants unless otherwise indicated.

Lutetium–Hafnium isotopes of selected U–Pb dated zircons were analyzed employing a Thermo NEPTUNE multi collector-inductively coupled plasma mass spectrometer (MC-ICPMS) at Goethe University Frankfurt. After column chemistry, the washes were dried down, redissolved in 250–400 μl 0.5 M HNO_3+0.1 M HF and transferred into pre-cleaned auto sampler microtubes. Solutions were introduced into the plasma employing an Aridus desolvation nebulizer with a nominal uptake rate of 100 μl/min. Isotopic ratios were measured in static mode on Faraday detectors equipped with 10^{10} (for mass 180) or 10^{11} (all other masses) resistors. ^{172}Yb, ^{173}Yb and ^{175}Lu were measured to correct for isobaric interferences of Yb and Lu on mass 176 assuming a $^{176}Yb/^{173}Yb$ ratio of 0.79502 and a $^{176}Lu/^{175}Lu$ ratio of 0.02656. Yb and Hf isotopic ratios were corrected for mass fractionation by normalizing to $^{172}Yb/^{173}Yb$ of 1.35351 and $^{179}Hf/^{177}Hf$ of 0.7325 using an exponential law. Mass fractionation of Lu was assumed to follow that of Yb (see Gerdes and Zeh, 2006). Accuracy and reproducibility of this protocol were assessed by repeat analyses of 10 ppb JMC 475 standard solutions ($^{176}Hf/^{177}Hf$=0.282148 ± 5, 2SD, n=21) bracketing unknowns. Initial $^{176}Hf/^{177}Hf$ ratios and εHf were calculated using the $^{206}Pb/^{238}U$ date of the respective crystal and the CHUR parameters of Bouvier et al. (2008); 176Lu/177Hf=0.0336; 176Hf/177Hf=0.282785). All uncertainties are given at the 2σ level and include the reproducibility of the JMC 475 solution propagated by quadratic addition.

For in-situ oxygen isotope analyses, zircon crystals were available from samples SK-218, SH-428 and SK-88. Sample BZN only yielded ~10 zircons that we preferred to use for geochronology. Zircon crystals were mounted in epoxy resin, polished to expose grain interiors and gold coated. Cathodoluminescence imaging prior to analyses did not reveal distinct cores and rims (Appendix C). A subset of three individual zircons were pressed in indium metal and only lightly polished (~2–4 μm) to achieve required flatness and analyze outermost rims. Exposed zircon cores and lightly polished zircon faces were analyzed for oxygen isotopes employing a CAMECA ims 1270 secondary ion mass spectrometer (SIMS) at the University of California, Los Angeles (UCLA). Instrumental calibration and analytical methods were identical to those of Bindeman et al. (2010). Uncertainties were estimated from the reproducibility of repeat analyses of standard zircon AS3 measured during the respective analytical session.

4. Zircon crystallization in the Skaergaard intrusion

As zircon has only recently been employed in study of Skaergaard (and other similar mafic intrusions), we here provide a discussion of zircon saturation and its time (and temperature) of appearance during crystallization. At crystallization temperatures of 1200–1000 °C and low zirconium concentrations (10–130 ppm; Brooks, 1969; McBirney, 2002), zircon unlikely was a cumulus phase during crystallization of LS gabbros. However, throughout the Skaergaard intrusion, the final stages of crystallization are characterized by granophyric accumulations occurring either as segregations of primary gabbroic pegmatites throughout the intrusion, or as interstitial granophyre that comprises up to 50% of late-stage differentiates around the SH (Wager and Brown, 1968; Larsen and Brooks, 1994; Larsen and Tegner, 2006). Late-stage silica enrichment, achieved either by fractional crystallization or liquid immiscibility (e.g., Jakobsen et al., 2005; Holness et al., 2011), is accompanied by progressive Zr enrichment with concentrations of 300–800 ppm in evolved gabbroic pegmatites and up to 2000 ppm in related granophyres (Brooks, 1969; Larsen and Brooks, 1994; McBirney, 1989; Fig. 2), represented by our sample SK-218. Bulk SH ferrodiorites (similar to our sample SH-428) have 250–350 ppm Zr (Brooks, 1969; McBirney,
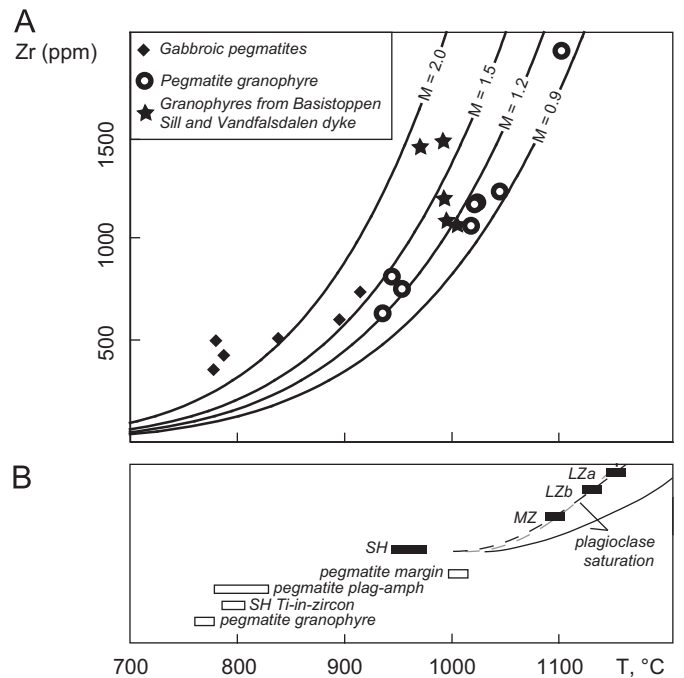

Fig. 2. Zircon saturation temperatures and crystallization temperatures of late-stage pegmatites and related granophyres. (A) Zr concentrations plotted against zircon saturation temperatures calculated according to Watson and Harrison (1983) using whole rock compositions published by McBirney (1989) and Larsen and Brooks (1994). (B) Independent constraints for the crystallization temperature of Layered Series gabbros (closed symbols and curves of plagioclase saturation temperature), late-stage pegmatites and related granophyres (open symbols; see text for details and references).

1989; McBirney, 2002) but interstitial granophyres are likely to be similar in composition to pegmatitic granophyres. We thus argue, that gabbroic pegmatites and evolved granophyres provide a good estimate for the range of compositions of zircon crystallizing interstitial liquids. Application of the zircon solubility model of Watson and Harrison (1983) returns apparent zircon saturation temperatures of 778–915 °C and 935–1102 °C for gabbroic pegmatites and related granophyres, respectively (Fig. 2). These zircon saturation temperatures have to be interpreted in the context of independent estimates for the formation temperatures of the respective mineral assemblages: gabbroic pegmatites experienced prolonged crystallization over a temperature interval from 1000 to 800 °C (Larsen and Brooks, 1994) and the granophyric assemblage crystallized close to the thermal minimum of the quartz-albite-orthoclase system (660–690 °C; Larsen and Tegner, 2006). Watson et al. (2006) reported Ti-in-zircon temperatures for zircons from the SH of 787–806 °C that are likely minimum temperatures due to undersaturation of these magmas in rutile. These data support that zircon was not a main cumulus phase but crystallized from silica enriched interstitial liquids. These late-stage silica enriched magmas formed at ~1000 °C and had near-liquidus zircon that crystallized over a narrow temperature interval from the time of zircon saturation until eutectic crystallization of the main granophyric assemblage.

The ~600 m thick Basistoppen Sill, a small layered intrusion in itself, had similar bottom to top crystallization and zircon saturation histories to Skaergaard. Upon differentiation, the Basistoppen Sill and related dykes (e.g., Vandfalsdalen dyke; White et al., 1989) achieved granophyric accumulations in the middle and towards the top, similar in composition to pegmatitic granophyres in the Skaergaard intrusion (Naslund, 1989; White et al., 1989). The main granophyric body related to crystallization of the Basistoppen Sill is the Sydtoppen granophyre on top of

Basistoppen, which has high radiogenic isotope ratios related to assimilation of Archean crust (Leeman and Dasch, 1978). Zr concentrations and calculated zircon saturation temperatures are similar to Skaergaard granophyres (Fig. 2; Naslund, 1989) indicating that zircon crystallization in the Basistoppen Sill is also associated with late-stage silica enrichment.

5. Oxygen isotope anatomy of the Skaergaard intrusion

Multitudes of bulk (whole rocks, bulk minerals) isotope analyses of oxygen and hydrogen isotopes are presented by Taylor and Forester (1979) and demonstrated profound and pervasive hydrothermal alteration by heated meteoric (rain and snow) water throughout the crystallization history of the intrusion. Plagioclase is particularly strongly altered and was used by Norton and Taylor (1979) to model time-integrated water–rock ratios for each volume of rock. Clinopyroxene shows less isotopic alteration where mineralogically unaltered and uninverted, and appears to indicate mantle-like values for the parental Skaergaard magma (Taylor and Forester, 1979). Clinopyroxene in more evolved rocks is extremely Fe-enriched (nearly pure hedenbergitic end-member; Brown and Vincent, 1963; McBirney, 2006), and is structurally and crystallographically represented by inverted ferrobustamite. It possesses consistently lower $\delta^{18}O$ values relative to coexisting plagioclase that were attributed to subsolidus inversion of magmatic ferrobustamite to a fine-grained mosaic of hedenbergitic clinopyroxenes, making them more susceptible to hydrothermal alteration. In order to circumvent these problems, Bindeman et al. (2008) performed single crystal analysis of least altered selected Skaergaard rocks with near magmatic $\Delta^{18}O_{plag\text{-}cpx}$, and also targeted refractory alteration resistant accessory phases (ferroamphibole, sphene, and zircon) that preserved primary magmatic $\delta^{18}O$ values and maintained $\delta^{18}O_{mineral\text{-}mineral}$ equilibrium characteristic of magmatic temperatures. These authors demonstrated that Skaergaard magma, coeval basalts, and the Basistoppen Sill initially were undoubtedly MORB-like, normal-$\delta^{18}O$ magmas, but evolved Skaergaard ferrodioritic rocks in the interior around SH crystallized from a low-$\delta^{18}O$ melt that was heterogeneously depleted by ~1 to 3‰ with respect to oxygen. However, the "$\delta^{18}O$ equilibrium" zircon value in the Sandwich Horizon is a less certain parameter. If we assume that large and unaltered sphene ($\delta^{18}O = 2.99 \pm 0.03$‰) represents the "true" solidus assemblage (and not high-T hydrothermal) as is texturally apparent, then using the fractionation factor $\delta^{18}O_{zircon\text{-}sphene} = 1.02$‰ (Valley et al., 2003), requires zircon to be 3.88‰ at 800 °C; if a 3‰ ferroamphibole is taken as a reference point, then the equilibrium zircon value is to be 3.28‰, similar to the bulk zircon measured. These $\delta^{18}O$ relationships suggest isotopic heterogeneities and motivated us to conduct a zircon oxygen isotope survey by ion-microprobe.

Individual ion microprobe oxygen isotope analyses of zircon cores and lightly polished crystal faces are given in Table 1 and are plotted in Fig. 3 together with previously published data (Taylor and Forester, 1979; Bindeman et al., 2008) against their stratigraphic position in the Skaergaard intrusion. Ion microprobe analyses revealed the presence of normal-$\delta^{18}O$ zircon cores throughout the Skaergaard intrusion. Note that because of the cooling and fractionation effects, the intercumulus or pegmatitic zircons are expected to be slightly lower in $\delta^{18}O$ than a canonical 5.3 ± 0.3‰ mantle zircon (e.g., Valley, 2003). This systematic shift to lower values is also consistent with slightly lower average clinopyroxene $\delta^{18}O$ values in Skaergaard (Fig. 3).

The newly observed differences between zircon core $\delta^{18}O$ values and those of bulk zircon fractions analyzed by laser fluorination (Bindeman et al., 2008) is interpreted to reflect inter- and intracrystalline heterogeneity and additional presence of

Table 1
Ion microprobe zircon oxygen isotope data. All $\delta^{18}O$ values are reported relative to Vienna Standard Mean Ocean Water (VSMOW).

Crystal/spot	core/face	$\delta^{18}O$ [‰], VSMOW	$\pm$ 1SD[a]
Sandwich Horizon ferrodiorites (SH-428; 13 crystals; 21 spots)			
SH428 1.1	c	4.82	0.47
SH428 1.2	c	4.11	0.47
SH428 2.1	c	4.62	0.47
SH428 2.2	c	5.34	0.47
SH428 3.1	c	4.76	0.47
SH428 3.2	c	4.33	0.47
SH428 3.3	c	4.12	0.47
SH428 3.4	c	4.11	0.47
SH428 3.5	c	4.02	0.47
SH428 4.1	c	5.38	0.47
SH428 4.2	c	4.29	0.47
SH428 4.3	c	4.90	0.47
SH428 5.1	c	5.38	0.47
SH428 6.1	c	4.20	0.47
SH428 7.1	c	4.83	0.22
SH428 8.1	c	4.95	0.22
SH428 9.1	c	4.61	0.22
SH428 10.1	c	4.72	0.22
SH428 11.1	f	3.80	0.36
SH428 12.1	f	3.97	0.36
SH428 13.1	f	3.64	0.36
Pegmatite in LZb (SK-218; 6 crystals; 8 spots)			
SK218 1.1	c	4.31	0.47
SK218 1.2	c	4.62	0.47
SK218 2.1	c	4.03	0.47
SK218 2.2	c	5.05	0.47
SK218 3.1	c	5.05	0.47
SK218 4.1	c	4.81	0.47
SK218 5.1	c	4.39	0.47
SK218 6.1	c	4.03	0.47
Sydtoppen granophyre (SK-88; 5 crystals; 5 spots)			
SK88 1.1	c	4.64	0.22
SK88 2.1	c	5.18	0.22
SK88 3.1	c	5.21	0.22
SK88 4.1	c	5.51	0.22
SK88 5.1	c	5.06	0.22

[a] 1 SD corresponds to the reproducibility of zircon standards analyzed during the same analytical session. Glass standards analyzed in the beginning of each session were reproducible to within 0.2–0.3‰.

isotopically light (~2‰) baddeleyite in bulk zircon fractions.[1] In the case of the pegmatite from LZb, zircon core and bulk zircon $\delta^{18}O$ values overlap suggesting that zircons are isotopically homogeneous within the resolution of SIMS analyses. Zircons from the Sydtoppen granophyre (SK-88) have average core $\delta^{18}O$ values that are ~0.5‰ higher than those of bulk zircon fractions. Isotopic heterogeneity is more pronounced in the most evolved part of the intrusion around the SH (sample SH-428). Ion microprobe analyses of zircon cores yielded $\delta^{18}O$ values ranging from 4.02 to 5.38‰ and lightly polished zircon crystal faces yielded $\delta^{18}O$ values of 3.64 to 3.97‰, similar to the lowest measured zircon core values, suggesting > 1‰ inter- and/or intracrystal variation with respect to $\delta^{18}O$. If baddeleyite contribution to bulk zircon analysis is ignored, then mass balance of 3.25‰ bulk zircon requires that individual (small) zircons or outermost several microns of some zircons had $\delta^{18}O$ values in ~1 to 2.5‰ range (Fig. 3B). These calculated rim values are similar to the 2‰ bulk zircons in sample KG-423 (Fig. 3), 30 m above SH. The ~2‰ $\delta^{18}O$ values are also in apparent isotopic equilibrium with many

---

[1] Baddeleyite in Skaergaard rocks appears as individual irregular shaped crystals and as inclusion within zircons (e.g., Fig. 4e in Bindeman et al., 2008). Small quantity of baddeleyite (0.12 mg) was analyzed as a mix with garnet standard by laser fluorination (see details in Appendix D) and yielded ~2.04 ± 1.12‰ value.
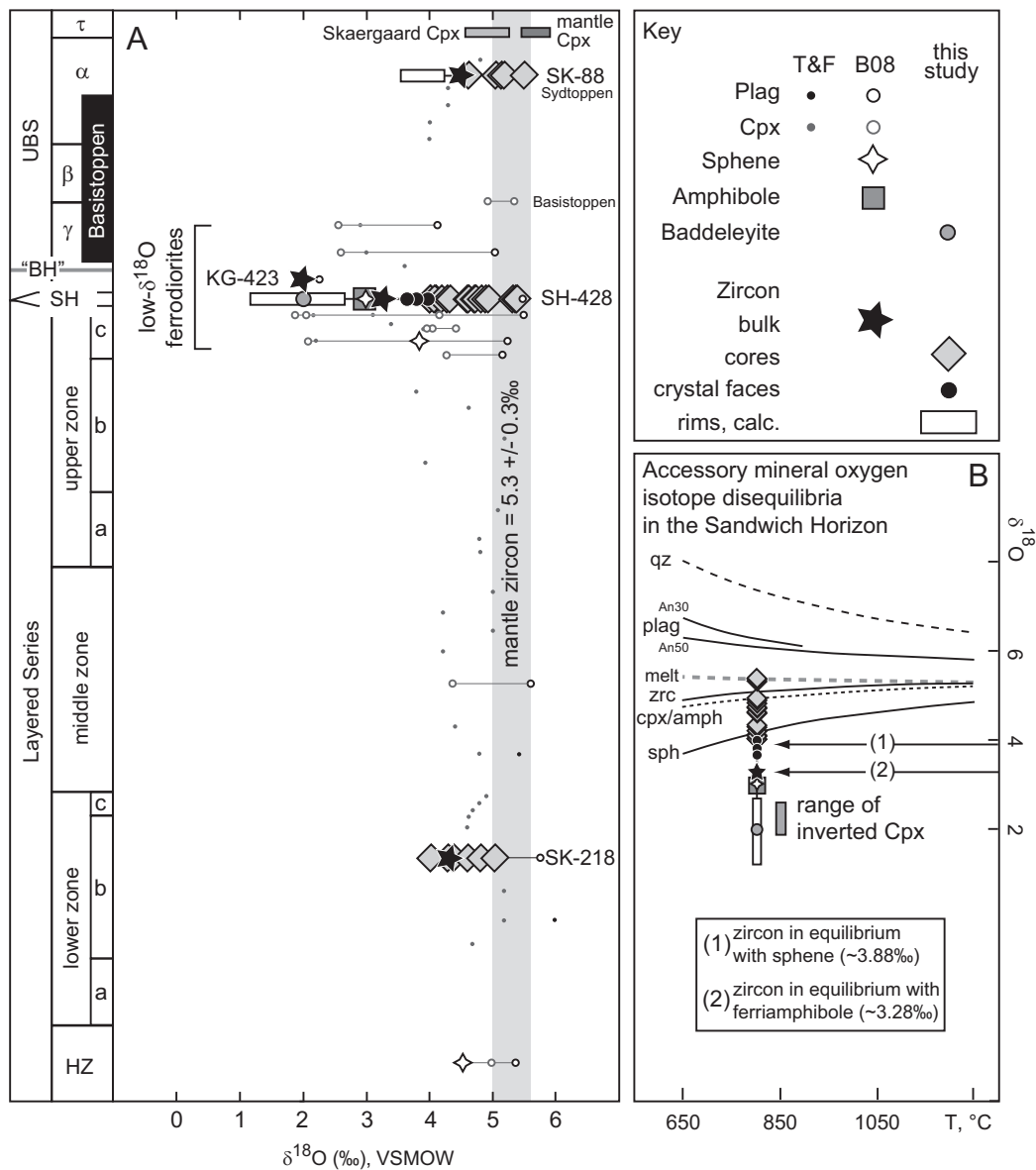
Fig. 3. Oxygen isotope anatomy of the Skaergaard intrusion. (A) $\delta^{18}O$ values of zircon cores and crystal faces analyzed by ion microprobe are plotted together with previously published oxygen isotope data of Taylor and Forester (1979) and Bindeman et al. (2008) against their stratigraphic position in the Skaergaard intrusion. (B) Illustration of accessory mineral oxygen isotope disequilibria in the Sandwich Horizon. Equilibrium oxygen isotope fractionation factors are plotted as a function of temperature for various minerals. $\delta^{18}O$ values of accessory minerals from the Sandwich Horizon are plotted at a plausible crystallization temperature of ~800 °C showing that ^{18}O depletion exceeds the magnitude of depletion expected from equilibrium fractionation. Horizontal arrows show $\delta^{18}O$ values of zircon in equilibrium with sphene and ferroamphibole.

individual inverted clinopyroxenes around the Sandwich Horizon (Bindeman et al., 2008), but are lower than is required by sphene and ferroamphibole in the same sample (Fig. 3B).

Fig. 4 represents our view of the textural evolution and magmatic-hydrothermal history of the SH that demonstrates that this assemblage is better viewed as "metamorphic", in a sense that it never achieved 100% remelting, chemical, and isotopic equilibration. Samples 30 m apart (i.e., KG-423 and SH-428) have zircons that are different by 1.3‰ in $\delta^{18}O$. Instead we speculate below that the melting degree upon reheating by Basistoppen was significantly less than 50% and that $\delta^{18}O$ was equilibrated only locally.

6. ID-TIMS zircon U–Pb geochronology

Zircon U–Pb results are listed in Table 2 and Fig. 5A displays $^{206}Pb/^{238}U$ dates corrected for initial ^{230}Th disequilibrium in comparison to previously published dates for the Skaergaard intrusion.

Additionally, Lu-Hf isotopic data of selected dated zircons are listed in Appendix A (Table A-1) and Fig. 5B–D show εHf values plotted against the Th/U ratio of the respective zircon and previously published whole rock Nd and Sr isotope ratios (McBirney and Creaser, 2003). These measurements of Hf isotopic composition were performed on the same zircons, allowing additional fingerprinting of sources. They demonstrate that dated zircons of the LS pegmatite and SH of Skaergaard overlap in isotopic composition, while Basistoppen zircons require a more radiogenic, likely crustally contaminated parental magma.

Seven out of eight $^{206}Pb/^{238}U$ zircon dates of the gabbroic pegmatite from lower zone b of the layered series (SK-218) are equivalent with a weighted mean date of 55.960 ± 0.018 Ma (mean square of weighted deviates, MSWD=1.4). We interpret this date to reflect rapid crystallization of the pegmatite after accumulation of intercumulus melt. We also consider this oldest age as the closest approximation of Skaergaard intrusion. Norton and Taylor (1979) modeled the thermal evolution of the
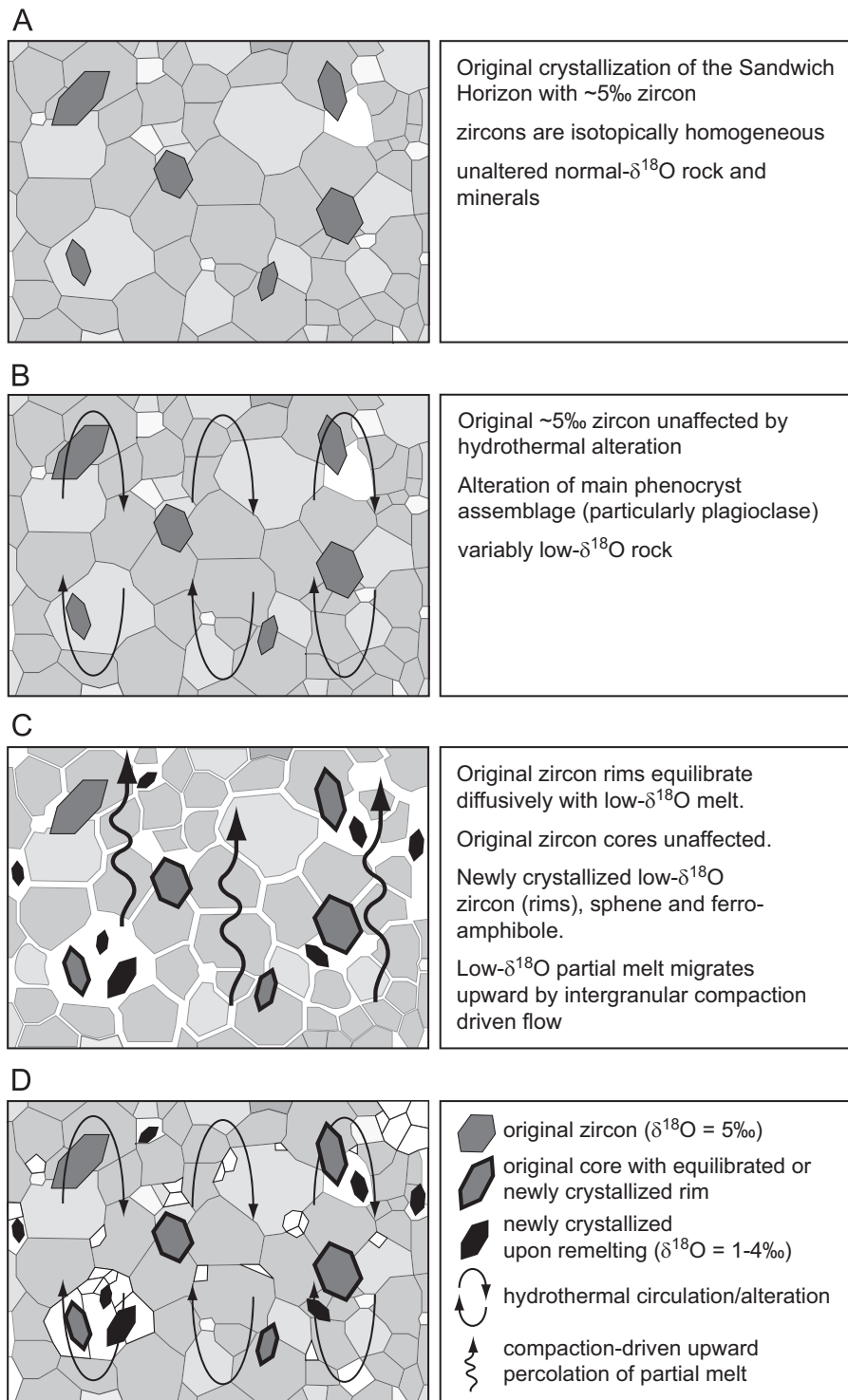
Fig. 4. Conceptual cartoon of accessory mineral behavior during crystallization and remelting of the Sandwich Horizon based on oxygen isotope heterogeneity. (A) Late-stage zircon crystallization from normal-δ^{18}O melt. (B) Variable hydrothermal alteration of main phenocryst assemblage leading to low-δ^{18}O whole rock, plagioclase and clinopyroxene values, while zircons are unaffected. (C) Reheating and partial remelting of hydrothermally altered Skaergaard differentiates leading to the formation of heterogeneously ^{18}O depleted magma, from which low-δ^{18}O zircon, sphene and ferroamphibole crystallize. Low-δ^{18}O melt is partially lost upwards by intergranular compaction driven flow. (D) Renewed hydrothermal alteration during slow plutonic cooling leaving low-δ^{18}O refractory minerals unaffected.

Skaergaard intrusion and estimated that cooling from 1200–1250 °C at the time of emplacement to 800–1000 °C, corresponding to the temperature of zircon saturation, took some 60 ka. Considering this model, the "true" intrusion age of Skaergaard can be estimated to be ~56.02 Ma. One SK-218 zircon yielded a significantly older ^{206}Pb/^{238}U date of 56.920 ± 0.085 Ma indicating minor xenocrystic or antecrystic contamination.

All analyzed zircons from the Basistoppen Sill (BZN; $n=8$) yielded statistically equivalent ^{206}Pb/^{238}U dates with a weighted mean of 55.895 ± 0.018 Ma (MSWD=0.51). As the sample was taken close to the contact with the Skaergaard intrusion, we consider this zircon crystallization age to approximate injection of the Basistoppen Sill. Notably, zircons from the Basistoppen Sill have distinctly higher Th/U ratios and are less radiogenic with respect to

Table 2
Zircon U–Pb isotopic results and calculated dates for samples from the Skaergaard intrusive complex.

Fraction[i]	Composition				Isotopic ratios								Dates (Ma)					
	Th/U [a]	Pb*(pg)[b]	Pbc (pg)[c]	Pb*/Pb$_c$ [d]	^{206}Pb/^{204}Pb [e]	^{206}Pb/^{238}U [f,g]	±2σ %	^{207}Pb/^{235}U [f]	±2σ %	^{207}Pb/^{206}Pb [f,g]	±2σ %	Corr.coef.	^{206}Pb/^{238}U [g]	±2σ abs	^{207}Pb/^{235}U [h]	±2σ abs	^{207}Pb/^{206}Pb [g]	±2σ abs
Basistoppen Sill (*BZN*)																		
BZN_z1	1.77	2.60	0.73	3.5	177	0.008707	0.19	0.0571	2.7	0.047579	2.6	0.753	55.89	0.10	56.4	1.5	78	61
BZN_z2	1.49	6.46	0.49	13.1	644	0.008710	0.12	0.05679	1.1	0.047288	0.99	0.694	55.903	0.065	56.08	0.58	64	23
BZN_z3	2.27	23.1	0.78	29.6	1230	0.008707	0.086	0.05667	0.42	0.047206	0.39	0.456	55.887	0.048	55.97	0.23	59.7	9.2
BZN_z4	1.35	2.49	0.45	5.5	290	0.008700	0.21	0.0567	2.9	0.047308	2.7	0.777	55.84	0.12	56.0	1.6	65	65
BZN_z5[j]	2.16	22.0	0.86	25.6	1090	0.008711	0.087	0.05718	0.51	0.047603	0.46	0.648	55.914	0.049	56.46	0.28	80	11
BZN_z6[j]	1.70	6.86	0.60	11.4	540	0.008706	0.097	0.05697	1.0	0.047462	0.97	0.333	55.879	0.054	56.26	0.55	73	23
BZN_z7[j]	1.82	10.8	0.50	21.7	979	0.008706	0.062	0.05662	0.52	0.047169	0.49	0.589	55.879	0.035	55.92	0.28	58	12
BZN_z8[j]	1.61	19.1	0.48	39.7	1866	0.008712	0.066	0.05672	0.36	0.047218	0.33	0.536	55.917	0.037	56.02	0.20	60.3	7.9
Sandwich Horizon (*SH-428*)																		
SH428_z1	1.08	3.90	0.63	6.2	341	0.008739	0.22	0.0570	2.0	0.047317	1.9	0.660	56.09	0.12	56.3	1.1	65	44
SH428_z2	0.55	8.94	0.58	15.4	936	0.008713	0.064	0.05676	0.44	0.047249	0.41	0.614	55.926	0.035	56.06	0.24	61.8	9.7
SH428_z3	1.33	7.42	0.85	8.8	451	0.008722	0.096	0.05637	1.0	0.046871	0.97	0.579	55.983	0.053	55.68	0.56	43	23
SH428_z4	0.71	3.08	0.60	5.1	309	0.008701	0.098	0.05712	1.4	0.047614	1.3	0.757	55.846	0.055	56.40	0.76	80	31
SH428_z5	0.64	7.98	0.49	16.4	970	0.008721	0.066	0.05704	0.45	0.047439	0.43	0.454	55.974	0.037	56.33	0.25	71	10
SH428_z6	0.63	2.50	0.53	4.7	288	0.008699	0.10	0.05767	1.6	0.048076	1.5	0.795	55.837	0.058	56.93	0.88	103	36
SH428_z7	0.46	7.83	0.59	13.2	821	0.008713	0.061	0.05708	0.50	0.047510	0.47	0.565	55.924	0.034	56.36	0.27	75	11
SH428_z8[j]	0.96	2.30	0.56	4.1	239	0.008714	0.13	0.0577	2.1	0.048061	2.0	0.810	55.932	0.071	57.0	1.1	102	46
SH428_z9[j]	0.96	21.4	0.41	51.9	2807	0.008714	0.036	0.05666	0.20	0.047153	0.17	0.717	55.932	0.020	55.96	0.11	57.0	4.2
SH428_z10[j]	0.45	7.79	0.39	19.9	1240	0.008700	0.042	0.05674	0.36	0.047303	0.36	0.233	55.839	0.023	56.04	0.20	64.5	8.5
SH428_z11[j]	0.74	8.38	0.42	20.1	1157	0.008715	0.049	0.05713	0.41	0.047542	0.37	0.764	55.937	0.027	56.41	0.22	76.6	8.9
SH428_z12	0.82	2.22	0.63	3.5	213	0.008697	0.12	0.0574	1.9	0.047875	1.8	0.833	55.820	0.064	56.7	1.1	93	44
SH428_z13	0.46	4.97	0.46	10.8	675	0.008712	0.076	0.05651	0.80	0.047040	0.75	0.677	55.918	0.042	55.81	0.43	51	18
SH428_z14	0.86	3.85	0.57	6.8	389	0.008713	0.082	0.05716	1.1	0.047575	1.0	0.755	55.925	0.046	56.44	0.58	78	24
SH428_z15	1.15	6.64	0.51	13.1	692	0.008711	0.075	0.05660	0.67	0.047122	0.63	0.527	55.914	0.042	55.90	0.36	55	15
SH428_z16	1.14	2.01	0.74	2.7	158	0.008699	0.17	0.0577	2.8	0.048142	2.7	0.858	55.837	0.093	57.0	1.6	106	63
Pegmatite in LZb (*SK-218*)																		
SK218_z1	0.79	13.5	0.85	15.8	902	0.008721	0.067	0.05728	0.56	0.047636	0.52	0.666	55.977	0.038	56.56	0.31	81	12
SK218_z2	1.19	3.00	0.74	4.0	223	0.008725	0.17	0.0564	2.3	0.046855	2.2	0.779	55.998	0.094	55.7	1.2	42	51
SK218_z3	0.79	19.3	0.82	23.6	1341	0.008715	0.062	0.05681	0.32	0.047278	0.30	0.491	55.940	0.035	56.11	0.18	63.3	7.0
SK218_z4	0.74	6.86	0.73	9.3	548	0.008717	0.094	0.05723	0.84	0.047619	0.79	0.556	55.950	0.052	56.51	0.46	80	19
SK218_z5	0.63	10.8	0.80	13.5	804	0.008723	0.071	0.05707	0.61	0.047450	0.57	0.600	55.988	0.040	56.35	0.33	72	14
SK218_z6	0.47	7.48	0.80	9.3	584	0.008710	0.11	0.05689	0.82	0.047375	0.77	0.573	55.903	0.059	56.18	0.45	68	18
SK218_z7	0.40	1.87	0.50	3.7	248	0.008719	0.12	0.0573	1.8	0.047654	1.7	0.839	55.965	0.065	56.57	0.99	82	40
SK218_z8	0.52	5.52	2.05	2.7	179	0.008869	0.15	0.0589	2.4	0.048127	2.3	0.853	56.920	0.085	58.1	1.4	106	54

[a] Th contents calculated from radiogenic ^{208}Pb assuming concordance between U–Th and Pb systems.
[b] Total mass of radiogenic Pb.
[c] Total mass of common Pb.
[d] Ratio of radiogenic Pb (including ^{208}Pb) to common Pb.
[e] Measured ratio corrected for fractionation and spike contribution only.
[f] Measured ratios corrected for fractionation, tracer and blank.
[g] Corrected for initial Th/U disequilibrium using radiogenic ^{208}Pb and Th/U[magma]=4±1 (2 s).
[h] Isotopic dates calculated using the decay constants λ_{238}=1.55125E−10 and λ_{235}=9.8485E−10 (Jaffey et al., 1971).
[i] Fractions are single crystals or fragments chemically abraded after Mattinson (2005).
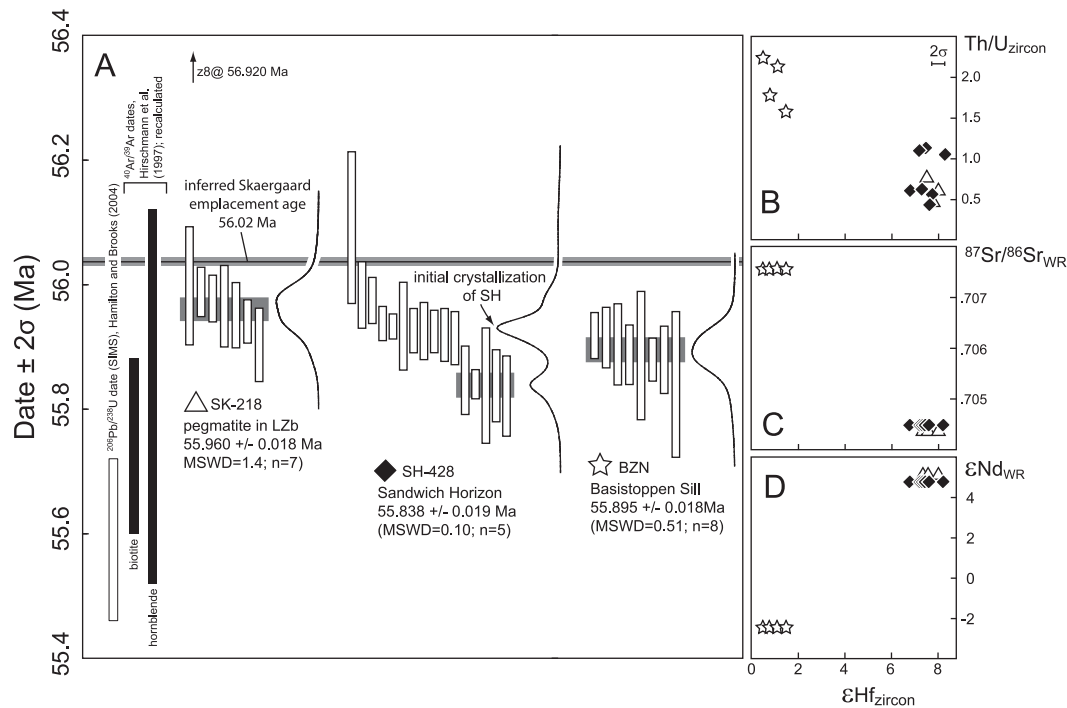[j] sample measured with ET2535 tracer.

Fig. 5. Geochronology of the Skaergaard intrusive complex. (A) Previously published ion microprobe U–Pb and $^{40}Ar/^{39}Ar$ dates of Hamilton and Brooks (2004) and Hirschmann et al. (1997), respectively and CA-ID-TIMS zircon dates for samples analyzed in this study, displayed as ranked ^{230}Th disequilibrium corrected $^{206}Pb/^{238}U$ dates with the weighted mean dates of the youngest populations and probability density distributions. (B-D) Hafnium isotope data of selected U–Pb dated zircons plotted against their Th/U ratio and whole rock Nd and Sr isotope data of McBirney and Creaser (2003). Note that $^{40}Ar/^{39}Ar$ dates of Hirschmann et al. (1997) were recalculated using the age of Kuiper et al. (2008) for the Fish Canyon sanidine standard and the ^{40}K decay constant of Min et al. (2000). All uncertainties are shown at the 95% confidence level.

$^{176}Hf/^{177}Hf$ than Skaergaard zircons, which coincides with elevated whole rock $^{87}Sr/^{86}Sr$ and less radiogenic Nd isotopic composition (Fig. 5B–D), indicating that they are autocrystic zircons and not antecrysts from the surrounding Skaergaard differentiates.

$^{206}Pb/^{238}U$ dates of zircons from the Sandwich Horizon (SH-428) range from 55.820 ± 0.064 to 56.09 ± 0.12 Ma. Many single grain dates do not overlap at the 95% confidence level (MSWD=6.6; $n=16$), precluding the calculation of a single weighted mean date for the population. We consider each single grain date to be accurate within the quoted uncertainty and regard the excess scatter to reflect protracted zircon growth. The oldest three zircon $^{206}Pb/^{238}U$ dates are slightly older than the crystallization age of the pegmatite from LZb. Another eight zircons define a subpopulation with $^{206}Pb/^{238}U$ dates that are younger than the pegmatite but older than the Basistoppen Sill. The remaining five zircons define a subpopulation with a weighted mean $^{206}Pb/^{238}U$ date of 55.838 ± 0.019 Ma that is 57 ± 37 ka younger than the intrusion age of the Basistoppen Sill (see discussion below).
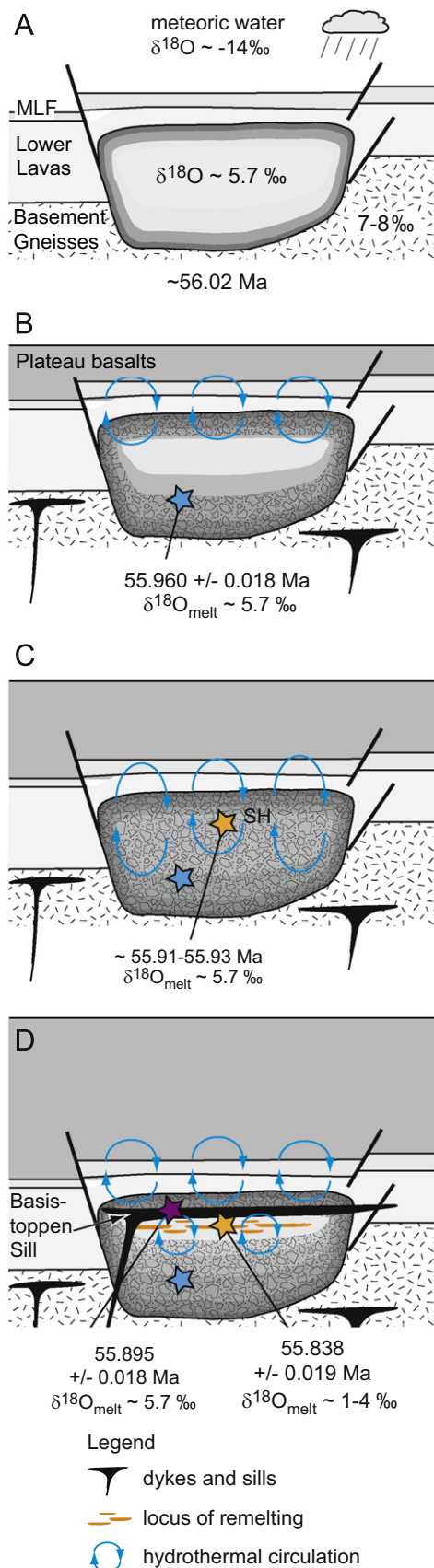
7. Discussion

7.1. In situ isotopic and geochronologic architecture of Skaergaard reveals partial remelting episode in its lifetime

Our new ion microprobe zircon oxygen isotope analyses and the high-resolution temporal framework derived from chemical abrasion ID-TIMS zircon geochronology provide critical new evidence that late-stage Skaergaard rocks became fully crystalline, hydrothermally altered, and subsequently partially remelted, induced by intrusion of the Basistoppen Sill (Fig. 6A–D). Ion microprobe analyses of zircon cores and zircon crystal faces from the Sandwich Horizon yielded $\delta^{18}O$ values, that are systematically higher than bulk zircon fractions, indicating that zircons in the most evolved part of the intrusion are zoned and isotopically heterogeneous in

$\delta^{18}O$. Furthermore, isotopic disequilibria between refractory minerals in this assemblage (zircon, sphene and ferroamphibole) suggest (1) heterogeneous hydrothermal depletion with respect to ^{18}O by $\sim 1–4‰$ relative to the initial mantle derived magma, consistent with centimeter scale $\delta^{18}O$ heterogeneity in other meteoric hydrothermal systems (e.g., Mora et al., 1999) and (2) incomplete reequilibration during partial remelting of these variably hydrothermally altered precursor rocks. Calculated minimum values of zircon rims or individual low-$\delta^{18}O$ zircons are also in apparent isotopic equilibrium with many inverted clinopyroxenes (fine grained hedenbergite mosaic; Lindsley et al., 1969) of the same or adjacent samples. Bindeman et al. (2008) speculated that these inverted low-$\delta^{18}O$ clinopyroxenes could be the result of remelting with high melt/solid ratios, whereupon these clinopyroxenes went through the crystallization cycle a second time, equilibrated with the low-$\delta^{18}O$ magma and inverted during cooling. Partial melting with low melt/solid ratios and solid-state recrystallization, in contrast, would result in large individual hedenbergite grains without the characteristic inversion textures (Bindeman et al., 2008). Isotopic equilibrium between some low-$\delta^{18}O$ zircons or zircon rims and inverted clinopyroxenes support this hypothesis and thus support models of remelting after subsolidus hydrothermal alteration.

Such a remelting event requires a proximal heat source and our new geochronological data contribute temporal relationships between late-stage crystallization of Skaergaard differentiates and emplacement of the Basistoppen Sill. Zircon crystallization ages for a normal-$\delta^{18}O$ pegmatite within LZb of the Layered Series and the Basistoppen Sill bracket initial solidification of the Skaergaard intrusion. The majority of zircons from the low-$\delta^{18}O$ SH is older than the crystallization age of the Basistoppen Sill (Fig. 5). We interpret this main population to record initial crystallization of the SH from a normal-$\delta^{18}O$ magma before intrusion of the Basistoppen Sill. The youngest five zircons define a population that is 57 ± 37 ka younger than the Basistoppen Sill (Fig. 5) suggesting that final solidification of the SH post-dates sill

Fig. 6. Cartoon summarizing the evolution of the Skaergaard intrusive complex. (A) Shallow emplacement of the Skaergaard intrusion into the unconformity between basement and overlying basalts. Estimated $\delta^{18}O$ of meteoric water ($-14‰$) is from Taylor and Forester (1979). (B) Progressive crystallization of the Skaergaard layered series (including pegmatite SK-218) from normal-$\delta^{18}O$ magma and initiation of a meteoric-hydrothermal system that primarily affects the Upper Border Series (UBS). (C) Initial crystallization of the Sandwich Horizon marks the complete solidification of the Skaergaard intrusion. The meteoric-hydrothermal system leads to alteration of most of the intrusion. (D) Intrusion of the Basistoppen Sill into UBS leads to reheating and partial remelting of surrounding Skaergaard differentiates. During these late stages of crystallization the Skaergaard intrusion is progressively buried by outpouring of the East Greenland flood basalts. Note that the thickness of basalts is not to scale.
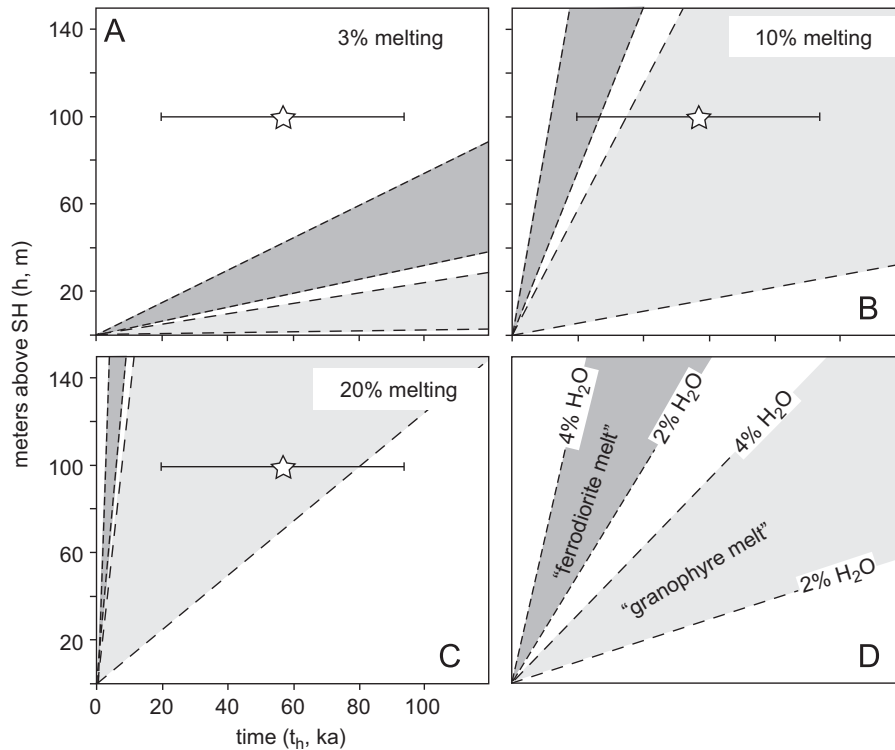
emplacement. This requires that the SH was remelted after subsolidus hydrothermal alteration by the Basistoppen Sill, in line with the oxygen isotope record. Together with our oxygen isotope results, these data suggest that remelting operated over quite some distance (>100 m) and not just along the contacts which is evident from the textural observation of local back-veining and hybridization (Naslund, 1989). Taking into account the possibility that the younger zircon population in the SH might correspond to zircons with post-Basistoppen overgrowth around older (i.e., >55.90 Ma) cores, the lag-time between intrusion of the Basistoppen Sill and crystallization of the youngest dated zircons from the SH may be regarded as a minimum time remelted SH spent above solidus. Considering the volumetric importance of zircon rims in bulk grain analyses and the relatively large uncertainty, we consider this lag-time as our best estimate for the duration of the remelting event (57 ± 37 ka).

7.2. Remelting and petrogenesis of the "Brooks" Horizon

The remelting model proposed for generation of late-stage Skaergaard differentiates (low-$\delta^{18}O$ magmas) might also provide an explanation for the petrogenesis of the so-called Brooks Horizon (or "secondary Sandwich Horizon", SHs, of McBirney, 2002), the most incompatible trace element-rich horizon in Skaergaard. The Brooks Horizon is located in UBSγ, approximately 100 m above SH and roughly coincides with the most ^{18}O depleted horizon in Skaergaard (Fig. 3). Partial remelting of hydrothermally altered rocks would produce ^{18}O depleted and trace element enriched melts. Accumulation of such melt at the Brooks Horizon requires upward percolation through the porous matrix during the remelting event, a process originally discussed by Irvine (1980). We calculated time scales of melt extraction from the partially molten porous matrix between the SH and the Brooks Horizon by compaction using algorithms of McKenzie (1984). Details of the calculation are given in Appendix B. As results of these calculations are most sensitive to the viscosity of the melt (e.g., Bachmann and Bergantz, 2004), which itself is a function of melt composition, we calculated two end-member scenarios: (1) for a melt equivalent in composition to SH ferrodiorites ("ferrodiorite melt") and (2) for a melt equivalent in composition to granitic granophyres ("granophyre melt"). For each melt composition, water content was varied between 2 and 4 wt%. Corresponding viscosities were computed using the model of Giordano et al. (2008). Fig. 7 shows the results of our calculations for various degrees of melting and compares computed time scales with the duration of the remelting event suggested by our geochronological data (i.e., 57 ± 37 ka). The calculations predict that low degrees of melting (e.g., 3%; Fig. 7A) are insufficient, as it would require >100 ka for melt migration from the SH to the Brooks Horizon. However, at higher degrees of melting (e.g., 10%; Fig. 7B), migration velocities are sufficiently high, except for the "dry granophyre melt", for melt migration by >100 m upwards from the SH during the remelting event. At $\sim20\%$ melting (Fig. 7C), computed time scales are shorter or within error of the duration of the remelting event, irrespective of

Fig. 7. Calculated time scales for melt migration from the Sandwich Horizon to the Brooks Horizon by compaction driven flow. (A)–(C) Calculations for various degrees of melting and different magma compositions with various H_2O contents. The star with uncertainty denotes the duration of the proposed remelting event derived from our geochronological data. (D) Graphical explanation for (A)–(C).

melt composition. Even higher degrees of remelting would be plausible around the SH where interstitial granophyre makes up to 50% of the rock. These simple calculations thus suggest that redistribution of trace elements by upward percolation of the most trace element rich melt formed during remelting is a plausible mechanism for explaining the petrogenesis of the Brooks Horizon.

7.3. Evolution of the Skaergaard intrusion and timing of related flood basalt volcanism

The Skaergaard intrusion is intimately linked to the East Greenland flood basalt province that was erupted during initial opening of the North Atlantic. It was always accepted that Skaergaard intruded into a very shallow rift, as is dictated by low-$\delta^{18}O$ altering waters, and was independently confirmed by pressure estimates based on coexisting SiO_2 polymorphs (tridymite and quartz) and ferrobustamite within Skaergaard that indicate pressures of 0.6 ± 0.1 kbar at ~ 950–$980\ ^\circ C$ (Lindsley et al., 1969). These pressure estimates, however, are likely minimum values (Lindsley et al., 1969) and strongly depend on the identification of tridymite (see discussion in Larsen and Tegner, 2006). These constraints nevertheless indicate that Skaergaard was emplaced prior to the main phase of flood basalt volcanism that produced a > 6 km thick sequence of volcanic overburden. Geochemical correlations of the Skaergaard intrusion and lavas of the flood basalt sequence yield additional constraints for the relative timing of intrusion emplacement and basalt eruption. Andreasen et al. (2004) and Nielsen (2004) suggested that the Skaergaard intrusion is correlative with the upper Geikie Plateau Formation or the lower Skraenterne Formation (see Fig. 1). More recently, Jakobsen et al. (2010b) showed that the composition of plagioclase-hosted melt inclusions in troctolitic blocks, corresponding to the unexposed most primitive Skaergaard cumulates, is equivalent to basalts of the Milne Land Formation (MLF, see Fig. 1) suggesting that they were emplaced contemporaneously, consistent with

shallow emplacement of Skaergaard. Furthermore, Larsen and Tegner (2006) used quartz-hosted fluid inclusions in granophyres to show that the Skaergaard intrusion underwent continuous burial during late stages of crystallization due to thickening of the volcanic overburden. Granophyres in LZa formed at pressures equivalent to 2.4 ± 1.5 km of volcanic overburden above the roof of the intrusion, corresponding to the Lower Lavas and the Skaergaard-like MLF. Granophyres higher up in the Skaergaard intrusion (LZb, MZ and SH) formed at pressures corresponding to > 6 km of volcanic overburden above the intrusion, suggesting that the bulk of the East Greenland flood basalt sequence was erupted during the late stages of crystallization of the Skaergaard intrusion. Our zircon crystallization ages record the timing of granophyre formation in LZb (SK-218) and the SH (SH-428) and allow us to scale the pressure increase reported by Larsen and Tegner (2006) to the temporal framework of intrusion crystallization (Fig. 8). Granophyres in LZb already record elevated pressures. Assuming accuracy of the relative pressure estimates (see Larsen and Tegner, 2006), this suggests that our zircon crystallization age for pegmatite SK-218 (55.960 ± 0.064 Ma, including systematic uncertainties) is a precise minimum age for the onset of flood basalt volcanism.

7.4. Skaergaard intrusion, related flood basalt volcanism and the Paleocene–Eocene thermal maximum

Flood basalt volcanism during opening of the North Atlantic has been suggested as a potential trigger mechanism for early Eocene environmental perturbations referred to as the Paleocene–Eocene thermal maximum (PETM). The PETM corresponds to a significant negative carbon isotope excursion (3.5–4.5‰) recorded in marine and terrestrial sediments that is associated with pronounced global warming and mass extinction among benthic organisms (e.g., Sluijs et al., 2007). Despite considerable effort to correlate magmatic activity in the Northeast Atlantic and the PETM (Storey et al.,
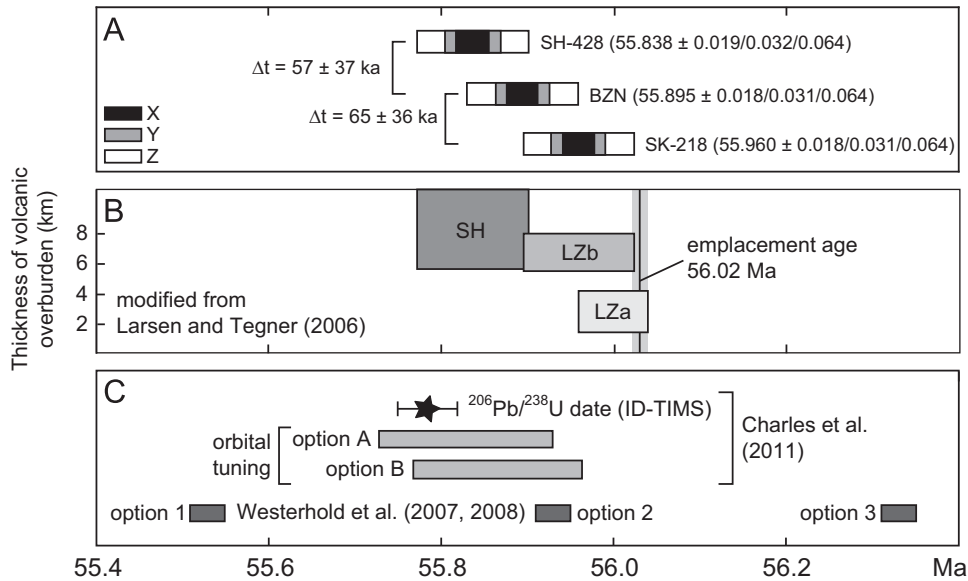
Fig. 8. Summary of Skaergaard geochronology and relation to the East Greenland flood basalts and the Paleocene–Eocene thermal maximum (PETM). (A) Weighted mean $^{206}Pb/^{238}U$ dates of analyzed samples from the Skaergaard intrusive complex. Dates are shown at different levels of uncertainty propagation: X—internal (analytical) uncertainty; Y—includes X and tracer calibration uncertainty; Z—includes X, Y and decay constant uncertainty. (B) thickness of volcanic overburden covering the Skaergaard intrusion from Larsen and Tegner (2006) schematically scaled to our Skaergaard zircon crystallization ages and (C) compilation of age estimates for the onset of the Paleocene–Eocene thermal maximum (Westerhold et al., 2007, 2008; Charles et al., 2011).

2007; Svensen et al., 2010), uncertainties on the order of ± 300 ka for lava flows, intrusions and sills are insufficient to confidently test synchronicity. In contrast, the onset of the PETM appears to be precisely constrained by cyclostratigraphy, although numerous tuning options have been proposed (Fig. 8). Recently, Charles et al. (2011) presented two options for the onset of the PETM based on orbital tuning relative to a $^{206}Pb/^{238}U$ zircon age of an ash bed within the PETM CIE. The youngest five zircons analyzed by Charles et al. (2011) yield a weighted mean $^{206}Pb/^{238}U$ date of 55.785 ± 0.034 Ma. This ash bed post-dates the onset of the PETM CIE by 40–80 ka, depending on the cyclostratigraphic interpretation. Consequently, Charles et al. (2011) derive ages of 55.829 ± 0.101 Ma or 55.866 ± 0.098 Ma (including systematic uncertainties) for the onset of the PETM. These estimates for the timing of the onset of the PETM overlap within uncertainty with our minimum estimate for the timing of flood basalt volcanism (55.960 ± 0.064 Ma, including systematic uncertainties; Fig. 8). We conclude that flood basalt volcanism associated with opening of the North Atlantic and the onset of the PETM are correlative at the < 100 ka level, strengthening models suggesting a causal link.

8. Summary and conclusions

[1] Based on our geochronology and a published cooling model we estimate the emplacement age of the Skaergaard intrusion to be ~56.02 Ma. Interstitial melt within the lower part of the intrusion reached zircon saturation by 55.960 ± 0.018 Ma and the final portions around the Sandwich Horizon crystallized at ~55.91–55.93 Ma (age of oldest peak in SH, see Fig. 4) suggesting that crystallization of ~300 km^3 of tholeiitic magma took some 100 ka.

[2] Intrusion of the Basistoppen Sill at 55.895 ± 0.018 Ma caused remelting of neighboring Skaergaard differentiates. The lag-time between intrusion of the Basistoppen Sill and subsequent crystallization of neighboring Skaergaard differentiates at 55.838 ± 0.019 Ma suggests a duration of 57 ± 37 ka for the remelting event.

[3] The Skaergaard intrusion initially crystallized from a normal-$\delta^{18}O$ MORB-like magma. Oxygen isotope geochemistry of refractory accessory minerals, particularly zircon, reveal that late-stage differentiates of the Skaergaard intrusion crystallized from a low-$\delta^{18}O$ melt that was heterogeneously depleted by 1–4‰ with respect to ^{18}O relative to the mantle derived precursor. Our high-precision zircon U–Pb geochronology suggest that shortly after initial solidification and subsequent meteoric-hydrothermal alteration, the newly intruded and hot Basistoppen Sill triggered partial remelting of the hydrothermally altered Skaergaard differentiates leading to the formation of low-$\delta^{18}O$ melts.

[4] This proposed remelting event may have also caused intergranular melt flow and redistribution of trace elements. Our simple calculations permit derivation of the Brooks Horizon, the most incompatible element-rich horizon in Skaergaard, by upward percolation of incompatible element-rich melt through the partially molten matrix during the remelting event.

[5] Our high-precision temporal framework for late-stage crystallization of the Skaergaard intrusion also provide time constraints for the eruption of intimately linked flood basalts, suggesting that flood basalt volcanism associated with opening of the North Atlantic is correlative with the Paleocene-Eocene thermal maximum at the < 100 ka level.

Appendix A. Supporting information

Supplementary data associated with this article can be found in the online version at http://dx.doi.org/10.1016/j.epsl.2012.08.043.

References

Andreasen, R., Peate, D.W., Brooks, C.K., 2004. Magma plumbing systems in large igneous provinces: inferences from cyclical variations in Palaeogene East Greenland basalts. Contrib. Mineral. Petrol. 147, 438–452.

Bachmann, O., Bergantz, G.W., 2004. On the origin of crystal-poor rhyolites: extracted from batholithic crystal mushes. J. Petrol. 45, 1565–1582.

Bindeman, I.N., Brooks, C.K., McBirney, A.R., Taylor, H.P., 2008. The low-δ^{18}O late-stage ferrodiorite magmas in the Skaergaard Intrusion: result of liquid immiscibility, thermal metamorphism, or meteoric water incorporation into magma? J. Geol. 116, 571–586.

Bindeman, I.N., Schmitt, A.K., Evans, D.A.D., 2010. Limits of hydrosphere-lithosphere interaction: origin of the lowest d^{18}O rocks on Earth in the Paleoproterozoic Karelian rift. Geology 38, 631–634.

Boudreau, A.E., McBirney, A.R., 1997. The Skaergaard Layered Series. Part III. Non-dynamic layering. J. Petrol. 38, 1003–1020.

Bouvier, A., Vervoort, J.D., Patchett, P.J., 2008. The Lu-Hf and Sm-Nd isotopic composition of CHUR: constraints from unequilibrated chondrites and implications for the bulk composition of terrestrial planets. Earth Planet. Sci. Lett. 273, 48–57.

Bowring, J.F., McLean, N.M., Bowring, S.A., 2011. Engineering cyber infrastructure for U–Pb geochronology: tripoli and U–Pb_Redux. Geochem. Geophys. Geosyst. 12 (6), http://dx.doi.org/10.1029/2010GC003479.

Brooks, C.K., 1969. On the distribution of zirconium and hafnium in the Skaergaard intrusion, East Greenland. Geochim. Cosmochim. Acta 33, 357–374.

Brooks, C.K., Gleadow, A.J.W., 1977. A fission-track age for the Skaergaard intrusion and the age of the East Greenland basalts. Geology 5, 539–540.

Brooks, C.K., Larsen, L.M., Nielsen, T.F.D., 1991. Importance of iron-rich tholeiitic magmas at divergent plate margins: a reappraisal. Geology 19, 269–272.

Brown, G.M., Vincent, E.A., 1963. Pyroxenes from the late stages of fractionation of the Skaergaard intrusion, East Greenland. J. Petrol. 4, 175–197.

Charles, A.J., Condon, D.C., Harding, I.C., Pälike, H., Marshall, J.E.A., Cui, Y., Kump, L., Croudance, I.W., 2011. Constraints on the numerical age of the Paleocene-Eocene boundary. Geochem. Geophys. Geosyst. 12 (6), http://dx.doi.org/10.1029/2010GC003426.

Gerdes, A., Zeh, A., 2006. Combined U–Pb and Hf isotope LA-(MC-) ICP-MS analyses of detrital zircons: comparison with SHRIMP and new constraints for the provenance and age of an Armorican metasediment in Central Germany. Earth Planet. Sci. Lett. 249, 47–62.

Gerstenberger, H., Haase, G., 1997. A highly effective emitter substance for mass spectrometric Pb isotope ratio determinations. Chem. Geol. 136, 309–312.

Giordano, D., Russell, J.K., Dingwell, D.B., 2008. Viscosity of magmatic liquids: a model. Earth Planet. Sci. Lett. 271, 123–134.

Hamilton, M.A., Brooks, C.K., 2004. A precise U–Pb zircon age for the Skaergaard intrusion. Geochim. Cosmochim. Acta 68, A587.

Hirschmann, M., Renne, P.R., McBirney, A.R., 1997. ^{40}Ar/^{39}Ar dating of the Skaergaard intrusion. Earth Planet. Sci. Lett. 146, 645–658.

Holness, M.B., Stripp, G., Humphreys, M.C.S., Veksler, I.V., Nielsen, T.F.D., Tegner, C., 2011. Silicate liquid immiscibility within the crystal mush: late-stage magmatic microstructures in the Skaergaard intrusion, East Greenland. J. Petrol. 52, 175–222.

Humphreys, M.C.S., 2011. Silicate liquid immiscibility within the crystal mush: evidence from Ti in plagioclase from the Skaergaard intrusion. J. Petrol. 52, 147–174.

Irvine, T.N., 1980. Magmatic infiltration metasomatism, double diffusive fractional crystallization, and adcumulus growth in the Muskox intrusion and other layered intrusions. In: Hargreaves, R.B. (Ed.), Physics of Magmatic Processes. Princeton University Press, Princeton. N.J., pp. 325–383.

Irvine, T.N., Andersen, J.C.O., Brooks, C.K., 1998. Included blocks (and blocks within blocks) in the Skaergaard intrusion: geologic relations and the origins of rhythmic modally graded layers. Geol. Soc. Am. Bull. 110, 1398–1447.

Jaffey, A.H., Flynn, K.F., Glendenin, L.E., Bentley, W.C., Essling, A.M., 1971. Precision measurement of half-lives and specific activities of ^{235}U and ^{238}U. Phys. Rev. C4 (5), 1889–1906.

Jakobsen, J.K., Veksler, I.V., Tegner, C., Brooks, C.K., 2005. Immiscible iron- and silica-rich melts in basalt petrogenesis documented in the Skaergaard intrusion. Geology 33, 885–888.

Jakobsen, J.K., Veksler, I.V., Tegner, C., Brooks, C.K., 2010a. Crystallization of the Skaergaard intrusion from an emulsion of immiscible iron- and silica-rich liquids: evidence from melt inclusions in plagioclase. J. Petrol. 52, 345–375.

Jakobsen, J.K., Tegner, C., Brooks, C.K., Kent, A.J.R., Lesher, C.E., Nielsen, T.F.D., Wiedenbeck, M., 2010b. Parental magma of the Skaergaard intrusion: constraints from melt inclusions in primitive troctolite blocks and FG-1 dykes. Contrib. Petrol. 159, 61–79.

Krogh, T.E., 1973. A low contamination method for hydrothermal decomposition of zircon and extraction of U and Pb for isotopic age determination. Geochim. Cosmochim. Acta 37, 485–494.

Kuiper, K.F., Deino, A., Hilgen, F.J., Krijgsman, W., Renne, P.R., Wijbrans, J.R., 2008. Synchronizing rock clocks of Earth history. Science 320, 500–504.

Larsen, R.B., Brooks, C.K., 1994. Origin and evolution of gabbroic pegmatites in the Skaergaard intrusion, East Greenland. J. Petrol. 35, 1651–1679.

Larsen, R.B., Tegner, C., 2006. Pressure conditions for the solidification of the Skaergaard intrusion: eruption of East Greenland flood basalts in less than 300,000 years. Lithos 92, 181–197.

Leeman, W.P., Dasch, E.J., 1978. Strontium, lead, and oxygen isotope investigation of the Skaergaard intrusion, East Greenland. Earth Planet. Sci. Lett. 41, 47–59.

Lindsley, D.H., Brown, G.M., Muir, I.D., 1969. Conditions of the ferrowollastonite-ferrohedenbergite inversion in the Skaergaard intrusion, East Greenland. Mineral. Soc. Am. Spec. Publ. 2, 193–201.

Mattinson, J.M., 2005. Zircon U–Pb chemical abrasion ("CA-TIMS") method: combined annealing and multi-step partial dissolution analysis for improved precision and accuracy of zircon ages. Chem. Geol. 200, 47–66.

McBirney, A.R., 1989. The Skaergaard Layered Series: I. Structure and average composition. J. Petrol. 30, 363–397.

McBirney, A.R., 1995. Mechanisms of differentiation in the Skaergaard intrusion. J. Geol. Soc. London 152, 421–435.

McBirney, A.R., 2002. The Skaergaard Layered Series, Part VI: Excluded trace elements. J. Petrol. 43, 535–556.

McBirney, A.R., 2006. Igneous Petrology, third ed. Jones and Bartlett, Sudbury, MA 550p.

McBirney, A.R., Creaser, R.A., 2003. The Skaergaard layered series, Part VII: Sr and Nd isotopes. J. Petrol. 44, 757–771.

McBirney, A.R., Noyes, R.M., 1979. Crystallization and layering of the Skaergaard intrusion. J. Petrol. 20, 487–554.

McKenzie, D., 1984. The generation and compaction of partially molten rock. J. Petrol. 25, 713–765.

McKenzie, D., 2011. Compaction and crystallization in magma chambers: towards a model of the Skaergaard intrusion. J. Petrol. 52, 905–930.

McLean, N.M., Bowring, J.F., Bowring, S.A., 2011. An algorithm for U–Pb isotope dilution data reduction and uncertainty propagation. Geochem. Geophys. Geosyst. 12 (6), http://dx.doi.org/10.1029/2010GC003478.

Min, K., Mundil, R., Renne, P.R., Ludwig, K.R., 2000. A test for systematic errors in ^{40}Ar/^{39}Ar geochronology through comparison with U–Pb analysis of a 1.1-Ga rhyolite. Geochim. Cosmochim. Acta 64, 73–98.

Mora, C.I., Riciputi, L.R., Cole, D.R., 1999. Short-lived oxygen diffusion during hot, deep-seated meteoric alteration of anorthosite. Science 286, 2323–2325.

Naslund, H.R., 1989. Petrology of the Basistoppen Sill, East Greenland: a calculated magma differentiation trend. J. Petrol. 30, 299–324.

Nielsen, T.F.D., 2004. The shape and volume of the Skaergaard intrusion, Greenland: implications for mass balance and bulk composition. J. Petrol. 45, 507–530.

Norton, D., Taylor Jr., H.P., 1979. Quantitative simulation of the hydrothermal systems of crystallizing magmas on the basis of transport theory and oxygen isotope data; an analysis of the Skaergaard intrusion. J. Petrol. 20, 421–486.

Norton, D., Taylor Jr., H.P., Bird, D.K., 1984. The geometry and high-temperature brittle deformation of the Skaergaard intrusion. J. Geophys. Res. 89B, 10178–10192.

Schaltegger, U., Brack, P., Ovtcharova, M., Peytcheva, I., Schoene, B., Stracke, A., Marocchi, M., Bargossi, G.M., 2009. Zircon and titanite recording 1.5 million years of magma accretion, crystallization and initial cooling in a composite pluton (southern Adamello batholith, northern Italy). Earth Planet. Sci. Lett. 286, 208–218.

Schoene, B., Crowley, J.L., Condon, D.C., Schmitz, M.D., Bowring, S.A., 2006. Reassessing the uranium decay constants for geochronology using ID-TIMS U–Pb data. Geochim. Cosmochim. Acta 70, 426–445.

Schoene, B., Guex, J., Bartolini, A., Schaltegger, U., Blackburn, T.J., 2010. Correlating the end-Triassic mass extinction and flood basalt volcanism at the 100 ka level. Geology 38, 387–390.

Sláma, J., Košler, J., Condon, D.J., Crowley, J.L., Gerdes, A., Hanchar, J.M., Horstwood, M.S.A., Morris, G.A., Nasdala, L., Norberg, N., Schaltegger, U., Schoene, B., Tubrett, M.N., Whitehouse, M.J., 2008. Plešovice zircon—a new natural reference material for U–Pb and Hf isotopic microanalysis. Chem. Geol. 249, 1–35.

Sluijs, A., Bowen, G.J., Brinkhuis, H., Lourens, L.J., Thomas, 2007. The Palaeocene-Eocene Thermal Maximum super greenhouse: biotic and geochemical signatures, age models and mechanisms of global change. In: Williams, M. (Ed.), Deep-Time Perspectives on Climate Change: Marrying the Signal from Computer Models and Biological Proxies, (eds) Soc. Spec. Publ, Micropalaeo, pp. 323–349.

Storey, M., Duncan, R.A., Swisher, C.C., 2007. Paleocene–Eocene thermal maximum and the opening of the northeast Atlantic. Science 316, 587–589.

Svensen, H., Planke, S., Corfu, F., 2010. Zircon dating ties NE Atlantic sill emplacement to initial Eocene global warming. J. Geol. Soc. 167, 433–436.

Taylor Jr., H.P., 1968. The oxygen isotope geochemistry of igneous rocks. Contrib. Mineral. Petrol. 19, 1–71.

Taylor Jr., H.P., Epstein, S., 1963. ^{18}O/^{16}O ratios in rocks and coexisting minerals of the Skaergaard intrusion. J. Petrol. 4, 51–74.

Taylor Jr., H.P., Forester, R.W., 1979. An oxygen and hydrogen isotopic study of the Skaergaard intrusion and its country rocks: a description of a 55-Ma fossil hydrothermal system. J. Petrol. 20, 355–419.

Tegner, C., Thy, P., Holness, M.B., Jakobsen, J.K., Lesher, C.E., 2009. Differentiation and compaction in the Skaergaard intrusion. J. Petrol. 50, 813–840.

Valley, J.W., 2003. Oxygen isotopes in zircon. Rev. Mineral. Geochem. 53, 343–385.

Valley, J.W., Bindeman, I.N., Peck, W.H., 2003. Empirical calibration of oxygen isotope fractionation in zircon. Geochim. Cosmochim. Acta 67, 3257–3266.

Veksler, I.V., Dorfman, A.M., Borisov, A.A., Wirth, R., Dingwell, D.B., 2007. Liquid immiscibility and the evolution of basaltic magmas. J. Petrol. 48, 2187–2210.

von Quadt, A., Erni, M., Martinek, K., Moll, M., Peytcheva, I., Heinrich, C.A., 2011. Zircon crystallization and the lifetimes of ore-forming magmatic-hydrothermal systems. Geology 39, 731–734.

Wager, L.R., Brown, G.M., 1968. Layered Igneous Rocks. W.H. Freeman, San Francisco 588 p.

Wager, L.R., Deer, W.A., 1939. Geological investigations in East Greenland. III. The petrology of the Skaergaard intrusion, Kangerdlugssuaq, East Greenland. Medd. Groenl. 105, 352.

Watson, E.B., Harrison, T.M., 1983. Zircon saturation revisited: temperature and composition effects in a variety of crustal magma types. Earth Planet. Sci. Lett. 64, 295–304.

Watson, E.B., Wark, D.A., Thomas, J.B., 2006. Crystallization thermometers for zircon and rutile. Contrib. Mineral. Petrol. 151, 413–433.

Westerhold, T., Röhl, U., Laskar, J., Raffi, I., Bowles, J., Lourens, L.J., Zachos, J.C., 2007. On the duration of magnetochrons C24r and C25n and the timing of early Eocene global warming events: implications from the Ocean Drilling Program Leg 208 Walvis Ridge depth transect. Paleoceanography 22 , http://dx.doi.org/10.1029/2006PA001322.

Westerhold, T., Röhl, U., Raffi, I., Fornaciari, E., Monechi, S., Reale, V., Bowles, J., Evans, H.F., 2008. Astronomical calibration of Paleocene time. Palaeogeogr. Palaeoclimatol. Palaeoecol. 257, 377–403.

White, C.M., Geist, D.J., Frost, C.D., Verwoerd, W.J., 1989. Petrology of the Vandfalsdalen Macrodike, Skaergaard Region, East Greenland. J. Petrol. 30, 271–298.